Progress In Electromagnetics Research M, Vol. 62, 123–130, 2017

Investigation on Circularly Polarized Ring Dielectric Resonator Antenna for Dual-band Wireless Applications

Deepika Pathak[1, *], Sudhir K. Sharma[1], and Vivek S. Kushwah[2]

Abstract—In this article, design and analysis of a dual-band ring dielectric resonator based radiator with circular polarization features is explored. The presented ring DRA is excited with the help of a tilted modified square-shaped aperture. Two important attractive features of the present article are: (i) two radiating modes originated inside the ring DRA, i.e., $HEM_{11\delta}$ and $HEM_{12\delta}$ mode; (ii) tilted modified square aperture generates circular polarized (CP) wave in both the operating frequency bands. For verifying the simulated results, practical model of the proposed antenna has been fabricated and verified. Experimental outcomes display that the proposed radiator functions over dual frequency bands, i.e., 2.8–3.58 GHz and 5.5–5.92 GHz respectively. 3-dB axial ratio (AR) frequency ranges of the proposed radiator are 2.8–3.2 GHz and 5.85–6.0 GHz, respectively. These appearances make it appropriate for some important wireless applications such as wireless LAN (2.4/5.2 GHz) and WiMAX (2.5 GHz) applications.

1. INTRODUCTION

In the recent age of wireless communication, Dielectric Resonator is one of the most famous radiators at microwave frequency. It is due to its several important features such as nonappearance of metallic and surface wave losses, high radiation efficiency, high gain and ease of integration with Monolithic microwave integrated circuits (MMICs) [1]. Initially, the research on dielectric resonator based radiator was started in 1983 by Prof. Long and his research colleagues [2]. Dielectric resonator antennas (DRAs) are accessible in various shapes and sizes such as hemisphere, cylinder, triangle, rectangle, tetrahedron, and pentagon. In this article, we use cylindrical shape DRA because of its easy availability in common market and provision of three different modes, i.e., $TE_{\phi rz}$, $TM_{\phi rz}$ and $HEM_{\phi rz}$ [3].

Recently, the designs of antennas with multiband and circular polarization characteristics are widely focused by research community. It is because of its several advantages such as working of single antenna for different wireless applications and orientation independency between transmitter and receivers [4]. Multiband antennas also provide minimum interference with non-applicable frequency band. Currently, several researchers have reported multiband characteristics in the case of DRA. There are three important techniques available in literature for obtaining multiband characteristics in DRA. The first and an important technique is the usage of different exciting methods such as coaxial probe, psi-shaped (ψ) microstrip line, and circular patch along with annular ring shape microstrip line [5–7]. The second technique is related to the shape of DRAs. In order to obtain multiband operations, irregular pentagon- and hexagon-shaped DRAs have been used by Sharma and Brar [8] and Hamsakutty et al. [9], respectively. The third technique, i.e., integrated antenna is very famous nowadays because it is a very simple method and also provides independent control over different frequency bands [10, 11]. Sharma and Gangwar presented the combination of a dual-segment cylindrical DRA with annular ring shape microstrip line printed in order to obtain triple band operation [12]. Similarly, the same research

Received 27 September 2017, Accepted 6 November 2017, Scheduled 15 November 2017

* Corresponding author: Deepika Pathak (deepikapathak199026@gmail.com).

[1] Department of Electronics Engineering, Jaipur National University, Jaipur, Rajasthan, India. [2] Department of Electronics Engineering, Amity School of Engineering & Technology, Gwalior, India.

group proposed a hybrid radiator, which is the grouping of annular ring metallic line and cylindrical DRA for multiband applications [13]. Gangwar et al. proposed a hybrid triple-band cylindrical DRA with two broadsided mode excitation, i.e., $HEM_{11\delta}$ and $HEM_{12\delta}$ [14]. Gupta et al. proposed a new dual-band dielectric resonator based antenna, where the DRA with dual-band characteristics generates dual radiating modes, i.e., $HEM_{11\delta}$ and $HEM_{12\delta}$ [15]. Some researchers are also interested in the creation of circular polarization along with multiband operations. In 2014, Pan et al. proposed a dual-band cylindrical DRA with circular polarization characteristics. They have achieved the CP waves with the help of modified circular patch [16]. Recently, Sharma et al. proposed a hybrid radiator with dual-band and circular polarization characteristics. This aerial structure is very simple. However, it has low gain value at higher frequency band [17]. Different shape DRAs have also been utilized for the creation of CP wave inside it, such as comb-shaped DRA, spidron fractal DRA and stair-shaped DRA [18–20].

This article examines the design and analysis of a circularly polarized ring dielectric resonator antenna with dual-band characteristics. In the proposed antenna structure, a tilted modified square slot is used to excite the ring DRA. This type of aperture provides strong coupling to both $HEM_{11\delta}$ and $HEM_{12\delta}$ modes. Two rectangular stubs on two sides of the slot and perturbation on the opposite side create CP waves in both the operating frequency bands of the proposed radiator. Apart from introduction, the entire article is divided into four subsections. Sections 2 and 3 explain the proposed radiating structure and its analysis, respectively. Sections 4 and 5 focuse on the measured outcomes and final conclusion, respectively.

2. ANTENNA STRUCTURE

Geometrical arrangement of the proposed integrated radiating structure is presented in Figures 1(a) and 1(b). A triangular aperture is etched over a glass epoxy substrate with a permittivity 4.4 and loss tangent 0.02. A alumina material based cylindrical DRA has been stacked on the triangular aperture with the help of gum. Alumina material has dielectric constant 9.8 and loss tangent 0.002. Table 1 lists the optimized dimension of different parameters of the proposed radiator.

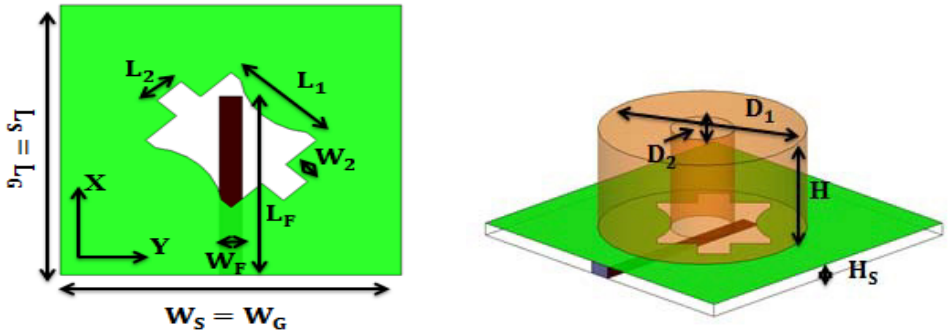

Figure 1. Geometrical layout of proposed integrated radiator. (a) Feeding mechanism, (b) 3D view.

Table 1. Dimension of different parameters of proposed integrated antenna.

Parameters	Dimension (mm)	Parameters	Dimension (mm)
L_G	40.0	L_F	22.0
$W_G = W_S$	40.0	L_1	10.0
D_1	26.0	L_2	4.5
H	13.0	W_F	2.7
H_S	1.6	W_2	4.5
D_2	8.0	L_S	40.0

3. ANTENNA ANALYSIS

This section explains the analysis of the proposed radiator, which includes accountability of different resonant elements towards different frequency bands as well as mechanism of CP wave generation. Ansoft HFSS based EM simulator has been used in order to optimized the proposed antenna structure. This section is separated into two subsegments: Section 3.1 dualband formation; Section 3.2 formation of CP wave.

3.1. Dual Band Generation

Figure 2 displays the $|S_{11}|$ variation with four different cases: (i) cylindrical DRA excited by using a square-shaped aperture; (ii) cylindrical DRA excited by a tilted square-shaped aperture; (iii) cylindrical DRA excited by a modified tilted square-shaped aperture; (iv) ring DRA excited by a modified tilted square-shaped aperture. In case-I, a cylindrical shape DRA is excited with the help of a square-shaped aperture. The square-shaped aperture always behaves as a magnetic dipole [4]. Therefore, it provides strong coupling to $\mathrm{HEM}_{11\delta}$ mode (lower band) with weak coupling to $\mathrm{HEM}_{12\delta}$ mode (upper band) [21]. These mode features will be proven later. In order to improve coupling in upper band, a square-shaped aperture is tilted to 45°, i.e., case-II. By tilting the square-shaped aperture, X-polarized and Y-polarized electric field lines become in the same strength. This process provides good coupling to both $\mathrm{HEM}_{11\delta}$ and $\mathrm{HEM}_{12\delta}$ modes. In order to obtain CP waves in the given antenna structure, the tilted square-shaped aperture is modified by adding stubs on two sides while perturbing on the other sides, i.e., case-III. After modification, there is no change in the $|\mathrm{S}_{11}|$ characteristics. Axial ratio mechanism will be discussed in the next subsection. In case-IV, we convert a cylindrical DRA into a ring DRA. The ring DRA has lower Q-factor than the cylindrical one. It is due to its lesser permittivity [22]. Therefore, the ring DRA provides wider impedance bandwidth than the cylindrical DRA. Figure 3 displays the reflection coefficient ($|S_{11}|$) variation with and without ring DRA. From Figure 3, it is confirmed that both the frequency bands are due to ring DRA. Figure 4 displays E-field variation on the ring DRA at 3.0 GHz and 5.8 GHz, respectively. From Figure 4, it is confirmed that $\mathrm{HEM}_{11\delta}$ and $\mathrm{HEM}_{12\delta}$ modes are created inside the ring DRA at 3.0 GHz and 5.8 GHz, respectively [23]. This can also be confirmed by the following mathematical formulation [24]:

$$f_{r,\mathrm{HE}_{11\delta}} = \frac{18.963 \times 10^8}{\pi D\sqrt{\varepsilon_e + 2}} \left[0.27 + 0.36\left(\frac{D_1}{4H_e}\right) + 0.02\left(\frac{D_1}{4H_e}\right)^2\right] \tag{1}$$

where,

$$\varepsilon_e = \frac{H_e}{\dfrac{H}{\varepsilon_{r,\mathrm{ring}}} + \dfrac{H_S}{\varepsilon_{r,\mathrm{sub}}}} \tag{2}$$

$$H_e = H + H_S \tag{3}$$

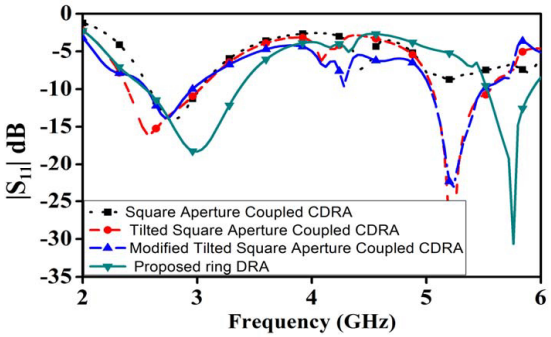

Figure 2. Variation in $|S_{11}|$ with different changes in antenna structure.

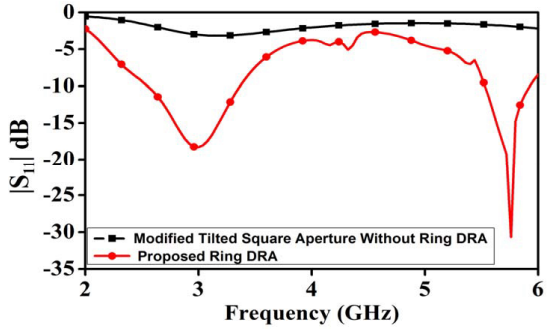

Figure 3. Variation in $|S_{11}|$ with and without ring DRA excited by proposed aperture.

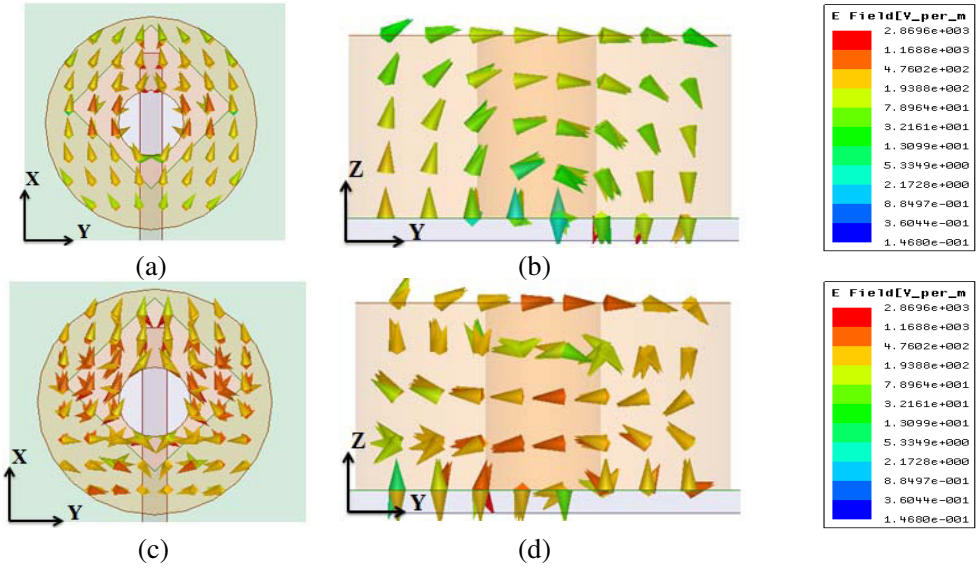

Figure 4. *E*-field distribution on ring DRA. (a) Top view at 3.0 GHz, (b) side view at 3.0 GHz, (c) top view at 5.8 GHz, (d) side view at 5.8 GHz.

$$\varepsilon_{\text{ring}} = \frac{\varepsilon_{\text{alumina}} \times \varepsilon_{\text{air}}}{\varepsilon_{\text{air}} + \left(\ln \dfrac{D_1}{D_2}\right) \varepsilon_{\text{alumina}}} \tag{4}$$

The resonant frequency of $\text{HEM}_{12\delta}$ mode is predicted with the help of resonant frequency of $\text{HEM}_{11\delta}$ mode. It is calculated as follow [21]:

$$f_{r,\text{HE}_{12\delta}} = 1.8 \times f_{r,\text{HE}_{11\delta}} \tag{5}$$

From Eqs. (1)–(5), the resonant frequencies of $\text{HEM}_{11\delta}$ and $\text{HEM}_{12\delta}$ modes are found to be 3.2 GHz and 5.76 GHz, respectively. They are quite close to the simulated resonant frequency.

3.2. Principle of CP Wave

For creating CP wave in any antenna structure, two conditions must be fulfilled: (i) creation of degenerated orthogonal modes; (ii) 90° phase shift between orthogonal modes [25]. These two necessary conditions are fulfilled by using some modification in the tilted square-shaped aperture. Figure 5 shows the modification in antenna structure in order to obtain the CP wave in both frequency bands.

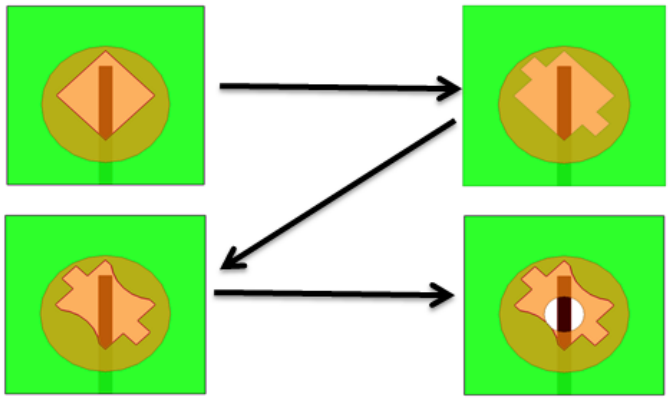

Figure 5. Different modification in proposed antenna structure in order to obtain CP wave.

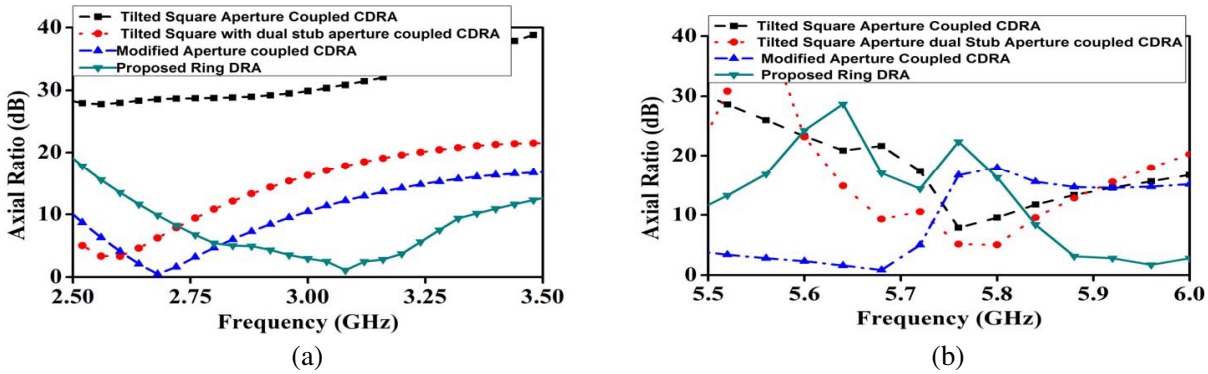

Figure 6. Axial ratio variation with respect to frequency. (a) Lower frequency band, (b) upper frequency band.

Figure 6(a) and Figure 6(b) display the axial ratio variation in lower and upper frequency bands. From Figure 6(a), it is clearly observed that rectangular stubs at the two opposite sides of tilted square aperture create dual degenerated orthogonal modes with 90° phase shift in lower frequency band (Phase Shift $= \frac{2\pi}{\lambda} \times$ Path delay) [26]. Similarly, perturbation on the two opposite sides produces CP wave in upper frequency band, shown in Figure 6(b). It is because of the orthogonal mode (in space) are accountable for upper and lower operating frequency bands. Ring DRA shifts the AR frequency to higher frequency, which is due to reduction in effective permittivity.

4. EXPERIMENTAL RESULTS

In this section, we experimentally verify the simulated outcomes and also focus on the far-field characteristics of the proposed radiator. For this purpose, we have fabricated the proposed antenna structure, shown in Figure 7. It is measured by using Keysight-based vector Network analyzer E5071C with a frequency range 9.0 kHz to 20 GHz. Figure 8 shows the measured and simulated reflection coefficient ($|S_{11}|$) variations with respect to frequency. From Figure 8, it can be observed that there is decent settlement between measured and simulated outcomes. Some difference is observed, which is due to the use of adhesive material for fixing the ring DRA. Table 2 shows the comparison of the proposed antenna structure with other published dual-band antennas on the basis of impedance bandwidth. From Table 2, it can be observed that the proposed structure provides better impedance bandwidth than others. As we can see, the impedance bandwidth in [13] in lower frequency band is better than the proposed antenna structure. However, [13] is based on hybrid antenna technique, which does not provide complete advantages of DRA, i.e., gain fluctuations are very high. The proposed radiator overcomes the drawback of hybrid radiators.

Figure 9(a) and Figure 9(b) show measured and simulated axial ratio variations with respect to

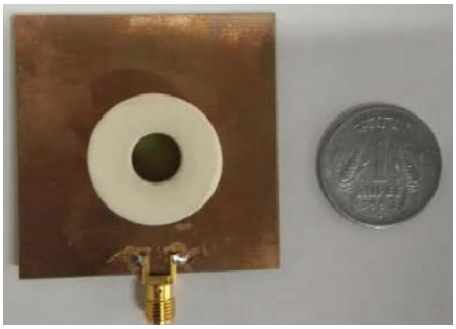

Figure 7. Photograph of fabricated antenna structure.

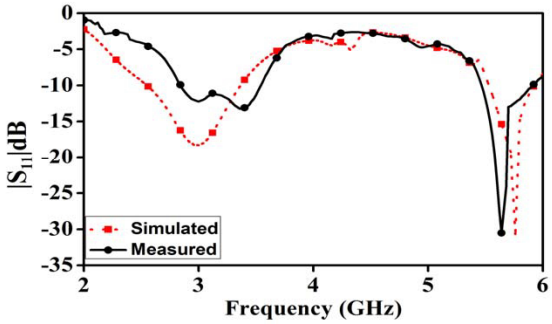

Figure 8. Measured and simulated variations in $|S_{11}|$ of proposed antenna structure.

Table 2. Comparison of proposed radiator with other published dual-band structure on the basis of impedance bandwidth.

Shape	Feed Type	Operating Freq. (GHz)	Lower (%)	Operating Freq. (GHz)	Upper (%)
Cylindrical [10]	Microstrip Line	2.36–2.5	3.3	5.4–5.8	5.7
Cylindrical [11]	CPW Feed	3.3–3.61	9	4.6–4.91	4.8
Cylindrical [17]	Slot	2.36–3.22	30.82	5.0–5.34	6.57
Ring (Proposed)	**Aperture**	**2.8–3.58**	**24.25**	**5.5–5.92**	**7.35**

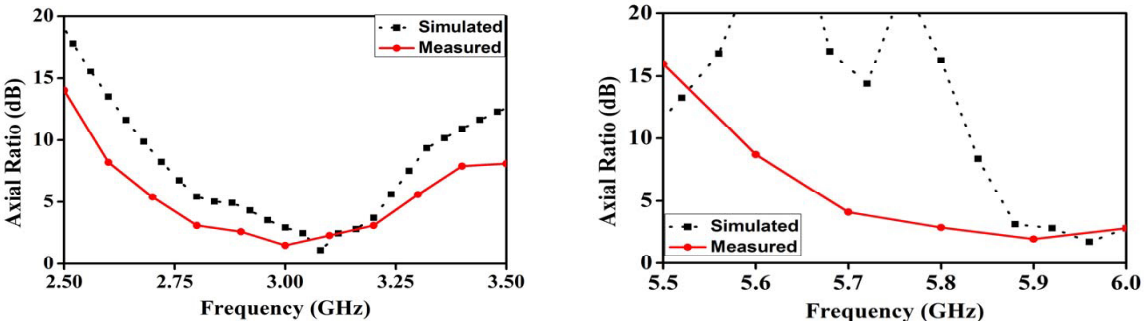

Figure 9. Measured and simulated axial ratio variation. (a) Lower frequency band, (b) upper frequency band.

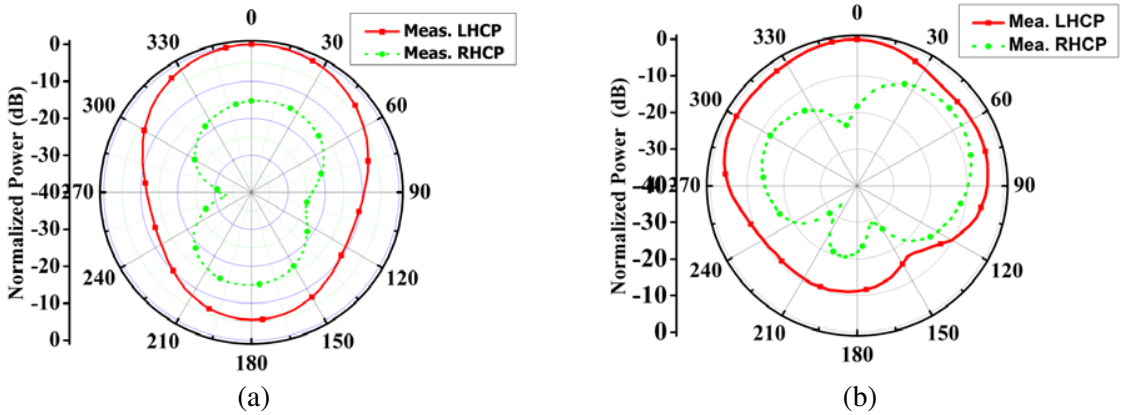

Figure 10. Measured LHCP/RHCP pattern. (a) 3.0 GHz, (b) 5.85 GHz.

frequency in lower and upper frequency bands, respectively. Axial ratio is measured in an anechoic chamber with the help of polarization pattern measurement technique [27]. There is good agreement between simulated and experimentally measured axial ratios. It is measured in the broadside direction ($\theta = 0°; \emptyset 0°$). From experimental results, 3-dB axial ratio frequency range of proposed radiator is found to be 2.8–3.2 GHz and 5.85–6.0 GHz, respectively. LHCP and RHCP patterns in XZ-plane at 3.0 GHz and 5.85 GHz are shown in Figure 10(a) and Figure 10(b), respectively. These patterns are measured in an anechoic chamber. LHCP and RHCP patterns are measured through the patterns in vertical and horizontal planes [28]:

$$E_{\text{RHCP}} = \frac{1}{\sqrt{2}}(E_H + jE_V) \tag{6}$$

$$E_{\text{LHCP}} = \frac{1}{\sqrt{2}}(E_H - jE_V) \tag{7}$$

From Figure 10, it can be said that the proposed radiator has a left-handed circularly polarized pattern in both the frequency bands. It is because of the more than 15 dB difference in between LHCP and RHCP towards broadside direction. Figure 11 displays the gain variation of the proposed radiator in broadside direction. The value of gain is higher in upper frequency band. It is due to the presence of $HEM_{12\delta}$ mode.

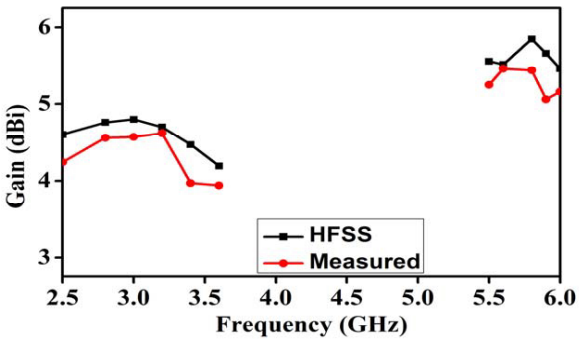

Figure 11. Gain (experimentally measured as well as simulated) variation with respect to frequency.

5. CONCLUSION

This paper explains the design analysis of a dual-band circularly polarized ring DRA for WLAN and WiMAX applications. It functions over dual frequency bands, i.e., 2.5–3.55 GHz and 5.5–5.92 GHz, respectively. Both the frequency bands are due to the ring-shaped dielectric resonator antenna. Two attractive characteristics of the proposed radiating arrangement are: (i) it supports dual hybrid modes, i.e., $HEM_{11\delta}$ and $HEM_{12\delta}$ modes, and emits maximum radiation in the broadside direction; (ii) it supports CP waves in both the operating bands, with simple modification in a square-shaped aperture. In both the working frequency bands, the proposed radiator supports left-handed circularly polarized wave.

REFERENCES

1. Petosa, A., *Dielectric Resonator Antenna Handbook*, Artech House, Norwood, MA, USA, 2007.
2. Long, S. A., M. W. McAllister, and L. C. Shen, "The resonant cylindrical dielectric cavity antenna," *IEEE Trans. Antennas Propag.*, Vol. 31, 406–412, 1983.
3. Luk, K. M. and K. W. Leung, *Dielectric Resonator Antenna*, Research Studies Press Ltd., Baldock, Hertfordshire, England, 2003.
4. Balanis, C. A., *Antenna Theory: Analysis and Design*, A John Wiley & Sons, Inc., 2005.
5. Hamsakutty, V., A. V. Praveen Kumar, G. Bindu, V. Thomas, A. Lonappan, J. Yohannan, and K. T. Mathew, "A multi frequency coaxial-fed metal coated dielectric resonator antenna," *Microwave Opt. Technol. Lett.*, Vol. 47, 573–575, 2005.
6. Sharma, A., G. Das, P. Ranjan, N. K. Sahu, and R. K. Gangwar, "Novel feeding mechanism to stimulate triple radiating modes in cylindrical dielectric resonator antenna," *IEEE Access*, Vol. 4, 9987–9992, 2016.
7. Sharma, A., P. Ranjan, and R. K. Gangwar, "Multiband cylindrical dielectric resonator antenna for WLAN/WiMAX application," *Electronics Letters*, Vol. 53, 132–134, 2017.
8. Sharma, S. K. and M. K. Brar, "Aperture coupled pentagon shaped dielectric resonator antennas providing multiband and wideband performance," *Microwave Opt. Technol. Lett.*, Vol. 55, 395–400, 2013.
9. Hamasakutty, V., A. V. Praveen Kumar, J. Yohannan, G. Bindu, and K. T. Mathew, "Co-axial fed hexagonal shaped dielectric resonator antenna for multi frequency operations," *Microwave Opt. Technol. Lett.*, Vol. 48, 887–880, 2006.

10. Chen, H. M., Y. K. Wang, Y. F. Lin, S. C. Lin, and S. C. Pan, "A compact dual-band dielectric resonator antenna using a parasitic slot," *IEEE Antennas Wireless Propag. Lett.*, Vol. 8, 173–176, 2009.
11. Li, Y. F., H. M. Chen, and C. H. Lin, "Compact dual-band hybrid dielectric resonator antenna with radiating slot," *IEEE Antennas Wireless Propag. Lett.*, Vol. 8, 6–9, 2009.
12. Sharma, A. and R. K. Gangwar, "Triple band dual segment cylindrical dielectric resonator antenna with a novel microstrip feed for wlan/wimax applications," *Microwave Opt. Technol. Lett.*, Vol. 57, 2649–2655, 2015.
13. Sharma, A. and R. K. Gangwar, "Tri-band hybrid cylindrical dielectric resonator antenna with hybrid mode excitation and cross-polarization suppression," *International Journal of RF and Microwave Computer Aided Engineering*, 2017, DOI: 10.1002/mmce.21130.
14. Gangwar, R. K., A. Sharma, M. Gupta, and S. Chaudhary, "Hybrid cylindrical dielectric resonator antenna with $HE_{11\delta}$ and $HE_{12\delta}$ mode excitation for wireless applications," *International Journal of RF and Microwave Computer Aided Engineering*, Vol. 26, 812–818, 2016.
15. Gupta, P., D. Guha, and C. Kumar, "Dielectric resonator working as feed as well as antenna: New concept for dual-mode dual-band improved design," *IEEE Trans. Antennas Propag.*, Vol. 64, 1497–1502, 2016.
16. Pan, Y. M., S. Y. Zheng, and W. Li, "Dual-band and dual-sense omnidirectional circular polarized antenna," *IEEE Antennas Wireless Propag. Lett.*, Vol. 13, 706–709, 2014.
17. Sharma, A., G. Das, and R. K. Gangwar, "Dual-band circularly polarized hybrid antenna for WLAN/WiMAX applications," *Microwave Opt. Technol. Lett.*, Vol. 59, 2450–2457, 2017.
18. Chu, L. C. Y., D. Guha, and Y. M. M. Antar, "Comb shaped circularly polarized dielectric resonator antenna," *Electronics Letters*, Vol. 42, 785–787, 2006.
19. Altaf, A., Y. Yang, K. Y. Lee, and K. C. Hwang, "Circularly polarized spidron fractal dielectric resonator antenna," *IEEE Antennas and Wave Propagation Letters*, Vol. 14, 1806–1809, 2015.
20. Fakhte, S., H. Oraizi, R. Karimian, and R. Fakhte, "A new wideband circularly polarized stair-shaped dielectric resonator antenna," *IEEE Trans. Antennas Propag.*, Vol. 63, 1828–1832, 2015.
21. Guha, D., P. Gupta, and C. Kumar, "Dual band cylindrical dielectric resonator antenna employing $HE_{11\delta}$ and $HE_{12\delta}$ mode excited by new composite structure," *IEEE Trans. Antennas Propag.*, Vol. 63, 433–438, 2015.
22. Sharma, A. and R. K. Gangwar, "Compact dual-band ring dielectric resonator antenna with moon-shaped defected ground structure for WiMAX/WLAN applications," *International Journal of RF and Microwave Computer Aided Engineering*, Vol. 26, 503–511, 2016.
23. Kajfez, D., A. W. Glisson, and J. James, "Computed modal field distributions for isolated dielectric resonators," *IEEE Trans. Antennas Propag.*, Vol. 32, 1609–1616, 1984.
24. Mongia, R. K. and P. Bhartia, "Dielectric resonator antennas-a review and general design relations for resonant frequency and bandwidth," *International Journal of Microwave and Millimeter-wave Computer Aided Engineering*, Vol. 4, 230–247, 1994.
25. Garg, R., P. Bhartia, I. Bahl, and A. Ittipiboon, *Microstrip Antenna Design Handbook*, Artech House, Norwood, MA, USA, 2001.
26. Kandasamy, K., B. Majumder, J. Mukherjee, and K. P. Ray, "Dual-band circularly polarized split ring resonators loaded square slot antenna," *IEEE Trans. Antennas Propag.*, Vol. 64, 3640–3645, 2016.
27. Stutzman, W. L. and G. A. Thiele, *Antenna Theory and Design*, A John Wiley & Sons, Inc., 2013.
28. Toh, B. Y., R. Cahill, and V. F. Fusco, "Understanding and measuring circular polarization," *IEEE Transactions on Education*, Vol. 46, 313–318, 2003.